Special Issue on "Theoretical and Computational Chemistry"

J. Indian Chem. Soc.,
Vol. 96, July 2019, pp. 767-774

QM/MM-MD simulation of the catalytic hydrolysis of L-captopril by microbial enzyme DapE

Debodyuti Dutta, Vipin Kumar Mishra and Sabyashachi Mishra*

Department of Chemistry, Indian Institute of Technology Kharagpur, Kharagpur-721 302, West Bengal, India

E-mail: mishra@chem.iitkgp.ac.in

Manuscript received online 22 April 2019, revised and accepted 08 May 2019

In the era of ever-increasing anti-microbial resistance, drug re-purposing offers a faster and economic route to the discovery of novel antibiotics. L-Captopril, a widely used angiotensin-converting enzyme inhibitor, has shown inhibitory action towards the microbial enzyme DapE, which is a potential antibiotic target. In this work, a series of biased and unbiased QM/MM-MD simulations has been carried out to investigate the catalytic hydrolysis of L-captopril along a general acid-base hydrolysis mechanism. The QM/MM-MD simulations not only provide an accurate estimation of free energy of activation, but also account for the corrections to the free energy arising from conformational dynamics of the enzyme-substrate complexes. The nucleophilic attack of the hydroxyl ion on the carbonyl group of L-captopril, was found to be the rate-determining step of the catalyzed hydrolysis reaction, which involved activation energy barrier of 15.6 and 13.1 kcal/mol, for the O- and S-coordinated conformations of L-captopril, respectively. Comparing these activation energy barriers with the barriers obtained for the hydrolysis of the natural substrate of DapE enzyme, it is concluded that the catalytic activation of L-captopril by DapE is as efficient as the activation of its natural substrate. Unlike the natural substrate, the activation of L-captopril by DapE yields side products that interrupt the crucial lysine biosynthetic pathway in bacteria.

Keywords: QM/MM-MD simulation, DapE enzyme, captopril inhibitor.

Introduction

The progress in electronic structure calculation has enabled quantum chemical treatment of large systems with chemical accuracy. However, a complete quantum mechanical (QM) treatment of biological systems, for example, an enzyme-substrate complex, is still prohibitively expensive from a computational point of view. On the other hand, the force-field based molecular mechanical (MM) treatment of these systems through classical (Newtonian) molecular dynamics methods is computationally affordable even for systems with close to a million particles[1], although the accuracy of these methods as well as their inability to describe bond breaking and bond formation limit their applicability to processes involving chemical reactions. To this end, the hybrid QM/MM approach overcomes the limitations of both QM and MM methods, by separating the large system into a small, yet chemically crucial part, to be treated with accurate and expensive QM methods and the remaining large part to be treated with MM method[2–5].

While the former allows the description of a chemical reaction, the latter provides the electrostatic environment necessary for the catalytic reaction to progress. With this strategy, the structural and enthalpic aspects of intermediates and transition states are computed in terms of the critical points in the multi-dimensional potential energy surfaces which provide crucial information to the mechanistic aspects of the enzyme catalysis. The QM/MM methods have found applications in a wide range of fields, from chemical biology to molecular physics to materials sciences. The relevance of the hybrid QM/MM approach to broad scientific community and to the society at large was acknowledged by the 2013 Nobel Prize in Chemistry to Warshel, Levitt, and Karplus, the pioneers of the field.

While the QM/MM approach can be used to describe the mechanistic details of a biochemical reaction by analyzing the structural and energetics aspects of the intermediates and the transition states of the reaction, a crucial aspect of any biochemical reaction that is ignored by conventional QM/MM approach is the underlying dynamics. Starting from Koshland's induced-fit model, the conformational dynamics in a large, flexible biomolecule has long been recognized to be important for the efficiency of the biochemical processes.

To account for the underlying dynamics, the QM/MM methods have been extended to QM/MM-MD method, where the time evolution of the hybrid QM/MM system is determined by following Newtonian trajectory in which the forces, obtained from the gradient of the potential energy, are evaluated for both QM atoms and MM atoms[6–10]. While QM/MM-MD simulations can be more insightful compared to the static QM/MM methods, it has been rarely performed for large biological systems due to the facts that these simulations are computationally very expensive and that, various QM/MM-MD methodologies are still under development. There are only a few studies reported which employ QM/MM-MD methodology and a majority of them generally employ semi-empirical methods to reduce the computational cost[11,12]. On the other hand, density functional theory based QM/MM-MD simulations have been rare, especially for reactive biomolecular systems[13–15].

In the present work, we report the structural, energetic, and dynamic aspects of catalytic action of a microbial enzyme employing the QM/MM-MD simulations. The microbial enzyme under consideration is the DapE-encoded N-succinyl-L,L-diaminopimelic acid desuccinylase (DapE), which has been shown to be indispensable for bacterial growth and multiplication, while absent in human host, thereby a potential source of antibiotic target with minimal side effects[16–18]. Given the endemic situation of bacterial infections and multi-drug resistance of several bacteria prevalent in Indian population, increasing level of research efforts need to be invested in the study of bacterial infection and their prevention. To this end, DapE enzyme is an ideal system for closer scrutiny of its catalytic action and its potential inhibitors.

The DapE enzyme catalyzes the hydrolysis of N-succinyl-L,L-diaminopimelicacid (L,L-SDAP) with high substrate specificity[19,20]. Over the last few years, our research group has studied this dimeric Zn containing enzyme by employing QM/MM calculations[21,22], MD simulations[23,24], QM/MM-MD simulations[25]. Our computational studies have resulted in a greater understanding of the catalytic action of this enzyme at atomistic level, not only in its wild-type form but also in several mutants of this enzyme.

Recent experimental studies have identified L-captopril as a competitive inhibitor of DapE enzyme, with a moderate inhibitory constant (K_i) of 1.8–2.8 μM[20,26,27]. L-Captopril is a well-known angiotensin-converting enzyme inhibitor and its inhibition of the completely unrelated DapE enzyme makes it a candidate for drug-re-purposing[27]. By extensive docking and MD studies, we have recently shown that L-captopril can bind the Zn centers of the DapE enzyme, either via its thiol group (S-coordination) or through its carboxylate group (O-coordination)[24]. Our calculations revealed that the O-coordination binding mode is thermodynamically favorable, while the S-coordination, the binding mode seen in the crystal structure, is kinetically favored[27]. Although, a detailed understanding of the mode of binding of this inhibitor is achieved from the crystal structure as well as from the computational studies, the mechanism of inhibition of the enzyme by L-captopril is not known. The present work aims to fill this gap. Herein, we investigate the possibility of activation of L-captopril by DapE enzyme, where we have considered both O- and S-coordination binding modes of the inhibitor and have carried out QM/MM-MD simulation to shed light on the mechanism of the catalytic action.

Computational methods

The starting structure of the L-captopril-bound DapE enzyme was taken from our previous study[24], where the binding modes of L-captopril with DapE enzyme have been investigated in great detail. In brief, the L-captopril molecule was docked in the DapE enzyme (PDB ID 3IC1)[28]. The docking analysis showed two major binding conformations of L-captopril to the metal centers of the enzyme. While the most populated binding mode showed coordination of L-captopril with Zn via its carboxylate group (O-coordination), a minor binding mode involved metal-ligand coordination via the thiol group (S-coordination)[24]. Both the conformations were considered for further processing, which involved a short minimization to overcome bad contacts, followed by 5 ns of heating and 5 ns of constant temperature and volume equilibration by employing Amber14 program[29]. The simulated system comprised of the enzyme-inhibitor complex solvated in an orthorhombic water box (90 Å×90 Å×100 Å) with appropriate number of sodium and chloride ions ensuring a charge neutral system as well as a salt concentration of 150 mM. The last snapshot of the equilibration was used for QM/MM-MD simulation.

To study the mechanism of catalytic hydrolysis of the L-captopril by DapE enzyme, we have employed a combination of biased and unbiased QM/MM-MD simulation techniques, similar to the methods employed in our earlier work[25].

In brief, the side chains of the active site residues of DapE (H67, D100, E135, E135, E163, H349), the two Zn ions, and L-captopril constituted the QM region whereas the remaining part of the protein and solvent served as the MM region. The atoms in the QM region were treated with the M06-2X functional[30] together with 6-31++G(d,p) basis set[31,32] where as the remaining atoms were described using Amber force field for protein and TIP3 potential for water molecules. The QM-MM interaction energy is calculated using electrostatic embedding scheme[33].

In a typical QM/MM-MD calculation, the forces acting on the atoms in a QM/MM calculation are given in terms of derivatives of the total energy with respect to the Cartesian coordinates of the atoms[10],

$$F = -\nabla E_{QM} - \nabla E_{MM} - \nabla E_{QM/MM} \quad (1)$$

The first two terms are the standard gradient expression for the QM energy and the classical MM force field energy that are used in the QM and MM regions, respectively. The forces acting on the QM atoms *A* and the MM atoms *k* due to the QM/MM interaction term are given by[10],

$$\nabla_A E_{QM/MM} = \sum_k^{N_{MM}} Q_k \int dr \frac{\nabla_A \rho_{QM}(r)}{|r - R_k|} + \sum_k^{N_{MM}} \nabla_A V_{AK}^{LJ} \quad (2)$$

$$\nabla_k E_{QM/MM} = Q_k \int dr \frac{\rho_{QM}(r) \times (R_k - r)}{|r - R_k|^3} + \sum_A^{N_{QM}} \nabla_k V_{AK}^{LJ} \quad (3)$$

where, V_{AK}^{LJ} is the Lennard-Jones potential between QM atom *A* and MM atom *k*, and ρ_{QM} is the QM charge density. From the above described forces, it is possible to either search for a minimum energy structure or to carry out MD simulations with QM/MM energy and forces by using standard computational techniques. The first derivative of the total energy, i.e. the sum of QM, MM, and QM-MM energies, with respect to the Cartesian coordinates of a given atom provides the force acting on the atom in the hybrid system, which is used to propagate the coordinates of the hybrid system, thus resulting in QM/MM-MD trajectories[10].

In this work, the QM/MM-MD trajectories were obtained at constant temperature (300 K) and pressure (1 bar). The Langevin dynamics with a Langevin thermostat was employed for obtaining constant temperature (300 K) and constant pressure (1 bar) was obtained by Berendsen barostat with a relaxation time of 1 ps. The particle mesh Ewald (PME) method was employed for the long-range electrostatic interactions between MM atoms with a 10 Å cutoff. All MM atoms that are found inside a 8 Å shell around any atom of the QM layer are considered in the nonbonding list of all QM atoms and the nonbonded interactions between the QM and MM atoms was treated with electronic embedding. SHAKE algorithm[34], was applied only on the hydrogen containing bonds in the MM layer and a time step of 0.5 fs was used. The non-equilibrium QM/MM-MD sampling was carried out using a combination of steered molecular dynamics (SMD) and umbrella sampling techniques[35] and the resulting umbrella sampling trajectories were analyzed using the weighted histogram analysis method (WHAM)[36,37] to obtain the free energy profile. All QM/MM-MD calculations were carried out using Amber14 program suite[29], with Gaussian 09[38] as an external program for QM calculations. 1 ps of the above QM/MM-MD simulation requires about 10 days of CPU time on a sixteen (Intel E52695 V2 2.4 GHz) core CPU. Employing the above computational methods, QM/MM-MD simulations were performed for the hydrolysis of L-captopril catalyzed by DapE enzyme following a general acid-base hydrolysis mechanism.

Results and discussion

L-Captopril has been shown to be a competitive inhibitor with K_i = 0.18–0.28 μM against microbial enzyme DapE[20,26,27]. From our previous studies, it is established that the inhibitor can have two binding modes, namely, the S-coordination and O-coordination (Fig. 1). While the former is kinetically favored, the latter is thermodynamically favored[24]. L-Captopril has an amide bond similar to that of SDAP (the natural substrate of DapE enzyme) that can be hydrolyzed by the DapE enzyme. In this section, we discuss the structural and energetic aspects of the catalytic hydrolysis of L-captopril in both S- and O-coordinated conformations by following a general acid-base hydrolysis reaction mechanism outlined in Fig. 2.

Activation of catalytic water molecule

Two snapshots were taken from the last nanosecond of the equilibration simulation of the O-coordinated as well as S-coordinated conformations and 5 ps unbiased QM/MM-MD simulations were carried out for each of these systems. In both the conformations, the catalytic water at the active site gets deprotonated by the Glu134 residue near the active site, as can be seen from the time series of the active site

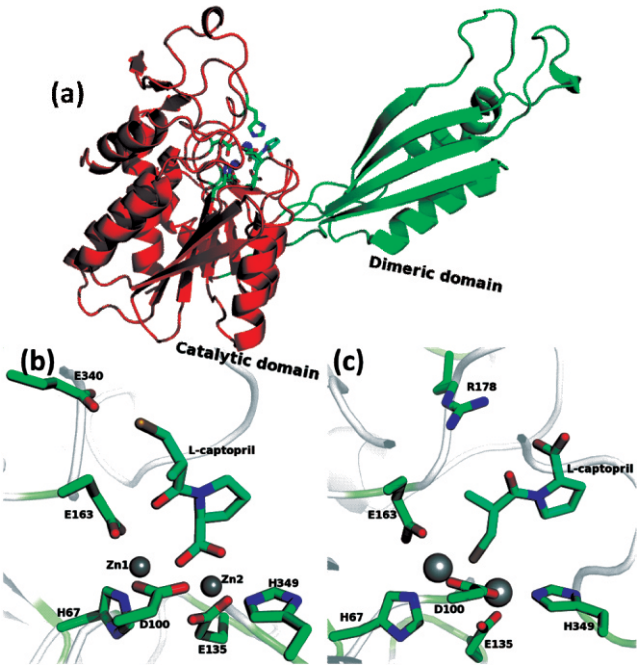

Fig. 1. (a) A cartoon representation of the catalytic and dimerization domain of DapE monomer. Active site of DapE enzyme bound to L-captopril via (b) O-coordinated and (c) S-coordinated binding modes.

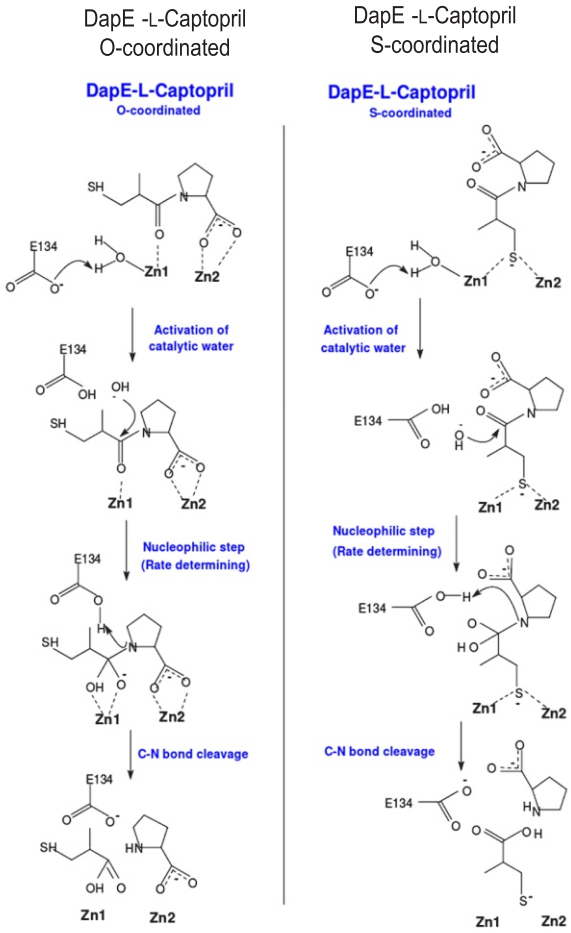

Fig. 2. Putative mechanism of the DapE catalyzed hydrolysis of L-captopril in O-coordinated and S-coordinated binding modes.

distances shown in Fig. 3a. It can be seen that the breaking of the O-H covalent bond in water and the formation of O-H bond in Glu134 occur simultaneously in all trajectories (Fig. 3a). While trajectory 1 in the O-coordinated L-captopril-DapE simulation showed a complete and irreversible proton transfer from the catalytic water to Glu134 at 2.5 ps of the QM/MM-MD simulation, the second trajectory showed a rather complex picture, with several iterations of transfer and back-transfer of proton before the final proton transfer from water to Glu134 at 3 ps of the QM/MM-MD simulation. After the completion of the proton transfer reaction, the resulting hydroxyl ion moves away from the Glu134 site, thus showing a larger separation of the OH^- group and the protonated Glu134 (Fig. 3). Similar observation is also made in the two QM/MM-MD trajectories started for the S-coordinated L-captopril-DapE complex. Here, both trajectories show proton transfer occurring around 3 ps of QM/MM-MD simulation. Unlike the trajectories obtained for O-coordinated L-captopril, in the S-coordinated L-captopril, both the trajectories showed a smaller separation between the resulting OH^- group and protonated Glu134. The QM/MM-MD snapshot at the instant of proton transfer was collected and an NBO analysis was performed at this geometry. It indicated a partially broken bond between the donor O atom and transferred proton as well as between the acceptor O atom and the transferred proton.

Since the proton transfer reaction is seen to proceed during the unbiased (equilibrium) QM/MM-MD simulation, the standard Boltzmann relation can be employed to estimate the free energy barrier between the reactant and product. The free-energy profile along the proton-transfer coordinate (r, the O-H distance of catalytic water) has been estimated from the probability distribution $P(r)$ in the QM/MM-MD simulation using the Boltzmann relation

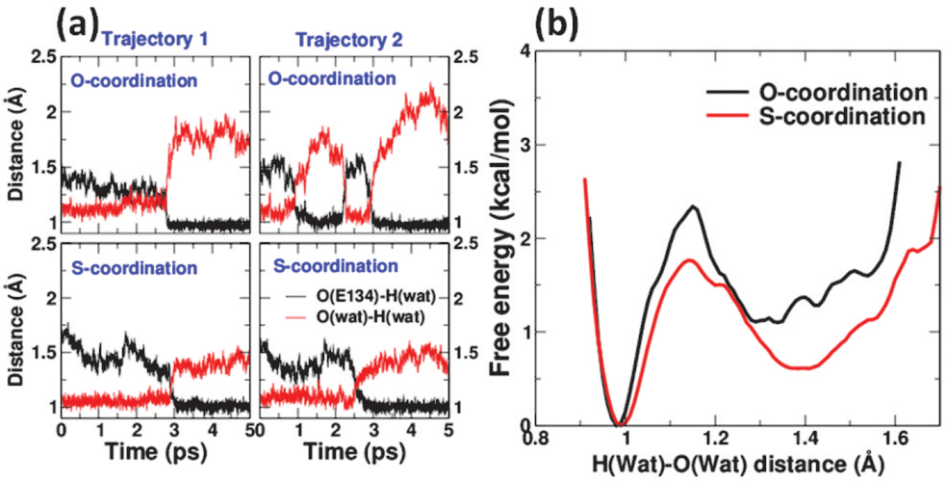

Fig. 3. (a) Time evolution of the reactive coordinates (distance between the proton and the proton acceptor (E134) in black and the distance between the proton and the proton donor (water) in red) during the activation of catalytic water molecule obtained from unbiased QM/MM-MD simulations when L-captopril is bound via O-coordination (upper panels) and S-coordination (lower panels) and (b) the corresponding free-energy profiles obtained from Boltzmann relation.

$$\Delta G(r) = -k_B T \ln P(r) \quad (4)$$

where, k_B is the Boltzmann constant and T is the temperature (300 K). The resulting free energy profiles show an activation energy barrier between 1.5 to 2.5 kcal/mol for the activation of the catalytic water molecule (Fig. 3b). The barrier estimated for the activation of the catalytic water molecule in the S-coordinated captopril is found to be marginally greater than that obtained for the O-coordinated mode of L-captopril. However, their difference (less than 1 kcal/mol) is too small to be differentiated by the present set of simulations.

Nucleophilic attack

From the above QM/MM-MD simulations, we observed that a substantial concentration of hydroxyl nucleophile is formed by deprotonation of the catalytic water molecule in both L-captopril conformations. The substrate hydrolysis reaction was further pursued for these systems. The formed hydroxyl ion undergoes a nucleophilic attack on the substrate's carbonyl group after the activation of the water molecule (Fig. 2). Our earlier QM/MM-MD investigation on the hydrolysis of SDAP estimated the activation energy barrier for the nucleophilic attack in the order of 15–20 kcal/mol, which amounts to a barrier too large to surmount during an unbiased QM/MM-MD simulation.

To sample such rare events, one often employs non-equilibrium methods, such as, umbrella sampling, steered molecular dynamics, or transition path sampling, etc. In a typical non-equilibrium sampling method, one carries out the desired process under some external guiding force, while ensuring to maintain a local equilibrium, to the extent possible, by carrying out the entire process in an infinite number of infinitesimally small steps. However, in practice, such a process is carried out in a finite number of small steps. This approximation, as expected, introduces error to the thermodynamic and kinetic quantities estimated from these simulations. However, the errors from these methods can be mitigated to a great extent by a careful choice of reaction coordinate and by carrying out multiple simulations.

The last snapshots of the unbiased QM/MM-MD trajectories, where the catalytic water is deprotonated resulting a hydroxyl ion, were taken as the starting snapshots from which QM/MM-steered MD (SMD) simulations were performed. Here the oxygen atom of the hydroxyl ion was moved towards the carbonyl carbon atom of the L-captopril by applying a force 100 kcal/mol/Å^2 along the chosen reaction coordinate. The NBO charge difference of the oxygen of the hydroxyl ion and the carbonyl carbon of L-captopril was found to be the largest after the catalytic water was deprotonated. Hence, the distance between the nucleophile and the electrophile was an obvious choice as the reaction coordinate for the nucleophilic attack. In our previous work, we have probed the effect of using different forces (100, 120,

150, and 200 kcal/mol/Å^2) and found that the results obtained from them are comparable.

As the hydroxyl ion moves closer to the carbonyl center of L-captopril, the protonated Glu134 also approaches the substrate with the progress of the QM/MM-SMD simulations, as it is hydrogen bonded to the hydroxyl ion. This can be seen from the time evolution of the active site distances (Fig. 4). The distance between the nucleophile and the carbonyl center is shorter in S-coordinated conformation of L-captopril, compared to that of the O-coordinated conformation. At the end of the SMD simulations, the hydroxyl group forms a covalent bond with the carbonyl carbon center of L-captopril and the carbonyl (C=O) double bond becomes a single bond. An NBO analysis of the last structure of the SMD trajectory confirms that the hybridization of the carbon center (the site of the nucleophilic attack), changes to sp^3 from an initial sp^2 hybridization.

From the above mentioned SMD simulations, once the path traversed by the nucleophile for the nucleophilic attack was obtained, snapshots at intervals 0.1 Å from the SMD trajectories were collected. This resulted in 29 snapshots for O-coordinated DapE-L-captopril system and 24 snapshots for S-coordinated DapE-L-captopril system. On each of these snapshots an umbrella potential (of 100 kcal/mol/Å^2 force constant) was applied along the nucleophile-substrate distance and 200 steps (100 fs) of umbrella sampling simulation was carried out. In our earlier work, we have benchmarked the employed force, as well as the selected intervals and the chosen length of simulation at each umbrella[25]. The (quasi) equilibrium QM/MM-MD simulations carried out for each umbrella potential was further analyzed to ensure sufficient overlap of the simulated structures between two neighbouring umbrella simulations. The resulting umbrella sampling trajectories were analyzed using weighted histogram analysis method (WHAM)[36,37] and the corresponding free-energy profiles are shown in Fig. 4. The free energy profiles from the WHAM analyses estimate the activation energy for the nucleophilic step as 15.6 and 13.1 kcal/mol for O-coordinated and S-coordinated conformations, respectively.

Cleavage of the amide bond

After the formation of the tetrahedral intermediate, the hydrolysis reaction of the substrate progresses through a transfer of protons from Glu134 to the nitrogen atom of the

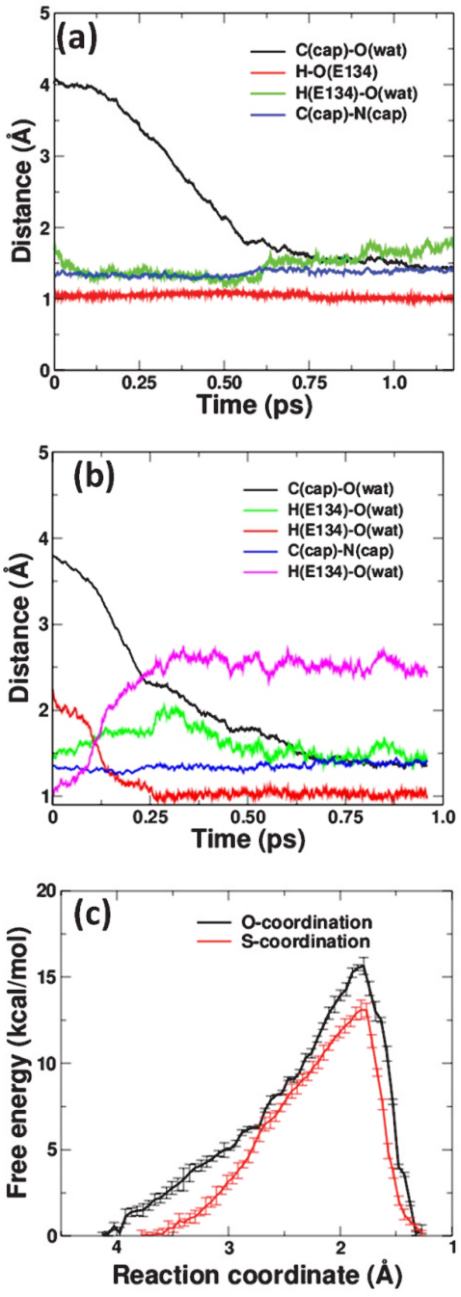

Fig. 4. (a) Time evolution of the reactive coordinates during QM/MM-SMD simulation of (a) O-coordinated and (b) S-coordinated DapE-L-captopril systems steered along the distance between the nucleophile (hydroxyl ion) and carbonyl carbon atom of L-captopril with a pulling force of 100 kcal/mol/A^2. The reaction coordinate could be traversed in 1.3 ps and 1 ps of non-equilibrium QM/MM-SMD simulations for the O-coordinated and S-coordinated systems, respectively. Captopril, catalytic water molecule, and Glu134 are indicated as cap, wat, and E134, respectively. (c) Free-energy profiles obtained from the weighted histogram analysis of the umbrella sampling trajectories.

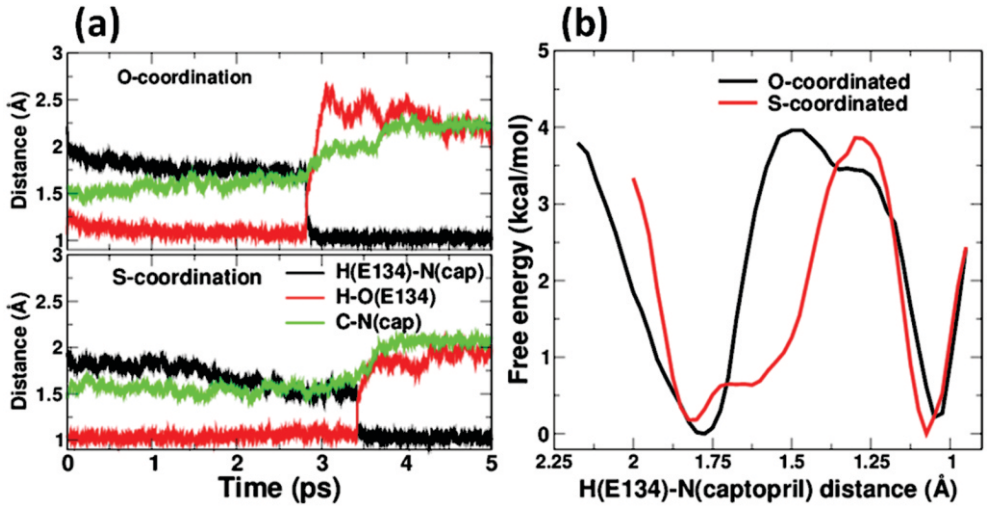

Fig. 5. (a) Time evolution of the reactive coordinates showing cleavage of the amide bond of L-captopril in O-coordinated (upper panel) and S-coordinated (lower panel) binding modes obtained from unbiased QM/MM-MD simulations of DapE-L-captopril systems with initial structure containing L-captopril in the tetrahedral intermediate form. (b) The free-energy profile along the proton transfer coordinate from the unbiased QM/MM-MD trajectories.

amide group of L-captopril, resulting in a weakening of the peptide bond that leads to the hydrolysis of the substrate (Fig. 2). The initial structure of the tetrahedral intermediate of the DapE-L-captopril complex was obtained by taking a snapshot from the last window of the umbrella sampling simulations for the nucleophilic attack. The tetrahedral intermediates in both O- and S-coordinated conformations of L-captopril, show a 2 Å distance between the carboxylate proton of Glu134 and the nitrogen of L-captopril. Similar to the activation of the catalytic water molecule, we performed another 5 ps unbiased QM/MM-MD simulation for both of these conformations. During the QM/MM-MD simulations, we observed proton transfer from Glu134 to the nitrogen atom of L-captopril (Fig. 5a), which leads to the cleavage of the C-N bond, thus completing the hydrolytic cleavage of L-captopril (Fig. 5a). In these simulations, breaking of the O-H covalent bond of the protonated side chain of Glu134 and formation of the N-H covalent bond was observed simultaneously, see Fig. 5a. The consequence of the proton transfer from Glu134 to the nitrogen of L-captopril is reflected in an increase in the C-N bond (Fig. 5a), which leads to the formation of the final product. The distance between C and N atoms (the atom of the cleaved C-N bond) is found to be between 2.1–2.3 Å in the present QM/MM-MD simulations. Since the molecules of the cleaved product are surrounded by the protein side chains in all directions, their movement is rather restricted.

Since the cleavage of the amide bond occurred during unbiased QM/MM-MD simulations, we employed Boltzmann's relation (eq. (4)) to estimate the activation energy barrier for this reaction step. The free energy profiles (Fig. 5b) show activation energy barrier of 4 kcal/mol for the cleavage of amide bond of L-captopril in both O- and S-coordinated conformations.

Conclusions

Using a combination of biased and unbiased QM/MM-MD simulations, the present work investigates the catalytic hydrolysis of L-captopril along a putative general acid-base hydrolysis mechanism. During the catalytic hydrolysis pathway, the nucleophilic attack of the hydroxyl ion (resulting from deprotonation of the catalytic water molecule by Glu134) on the carbonyl group of L-captopril was found to be the rate determining step involving an activation energy barrier estimated as 15.6 and 13.1 kcal/mol, for the O- and S-coordinated conformations, respectively. The activation energy barriers estimated in this work for the hydrolysis of L-captopril are comparable to those obtained for the catalytic hydrolysis of SDAP by DapE enzyme, in which the nucleophilic attack constituted the rate determining step with an activation energy barrier of 15.2 kcal/mol[25]. Taken together, this indicates that the catalytic activation of L-captopril by DapE is as efficient as the activation of the natural substrate. In fact, the

hydrolysis of S-coordinated L-captopril is calculated to be somewhat faster than the natural substrate SDAP. The products of the hydrolysis of SDAP (i.e., succinic acid and diaminopimelic acid) are extremely important for the continuation of the lysine biosynthetic pathway in bacteria. Hence, when DapE enzyme binds L-captopril, it readily cleaves it to give rise to hydrolysis products that are different from the hydrolysis product of the natural substrate. This prevents a further continuation of the lysine biosynthetic pathway in bacteria, which ultimately leads to the death of bacteria.

Acknowledgements

DD thanks IIT Kharagpur and VKM thanks CSIR, India for financial assistance. SM thanks DST-India, New Delhi for Ramanujan Fellowship and SERB, New Delhi for computational facility (EMR/2015/001890).

References

1. E. Tarasova and D. Nerukh, *J. Phys. Chem. Lett.*, 2018, **9**, 5805.
2. S. Ahmadi, L. Barrios Herrera, M. Chehelamirani, J. Hostas, S. Jalife and D. R. Salahub, *Int. J. Quantum Chem.,* 2018, **118**, e25558.
3. H. Lin and D. G. Truhlar, *Theor. Chem. Acc.*, 2007, **117**, 185.
4. A. Warshel and M. Levitt, *J. Mol. Biol.*, 1976, **103**, 227.
5. D. Bakowies and W. Thiel, *J. Phys. Chem.*, 1996, **110**, 10580.
6. D. Marx and J. Hutter, "Ab Initio Molecular Dynamics: Basic Theory and Advanced Methods", Cambridge University, Cambridge Press, 2009.
7. R. Car and M. Parrinello, *Phys. Rev. Lett.*, 1985, **55**, 2471.
8. D. Remler and P. A. Madden, *Mol. Phys.*, 1990, **70**, 921.
9. J. Hutter, "Car-Parrinello Molecular Dynamics", Wiley Interdisciplinary Reviews, Computational Molecular Science, 2012, **2**, 604.
10. A. W. Goetz, M. A. Clark and R. C. Walker, *J. Comput. Chem.*, 2014, **35**, 95.
11. H. C. Watanabe, M. Banno and M. Sakurai, *Phys. Chem. Chem. Phys.*, 2016, **18**, 7318.
12. L. Mones, A. Jones, A. W. Goetz, T. Laino, R. C. Walker, B. Leimkuhler, G. Csaenyi and N. Bernstein, *J. Comput. Chem.*, 2015, **36**, 633.
13. M. A. Nitsche, M. Ferreria, E. E. Mocskos and M. C. G. Lebrero, *J. Chem. Theory Comput.*, 2014, **10**, 959.
14. J. Torras, *Phys. Chem. Chem. Phys.*, 2015, **35**, 9959.
15. G. V. Dhoke, M. D. Davari, U. Schwaneberg and M. Bocola, *ACS Catal,* 2015, **5**, 3207.
16. G. Scapin and J. S. Blanchard, *Adv. Enzymol.*, 1998, **72**, 279.
17. T. L. Born and J. S. Blanchard, *Curr. Opin. Chem. Biol.*, 1999, **3**, 607.
18. D. Gillner, D. Becker and R. Holz, *J. Biol. Inorg. Chem.*, 2013, **13**, 155.
19. R. C. Holz, D. L. Bienvenue, D. M. Gilner, R. S. Davis and B. Bennett, *Biochemistry,* 2003, **42**, 10756.
20. N. Cosper, D. Bienvenue, J. Shokes, D. Gilner, T. Tsukamoto, R. Scott and R. Holz, *J. Am. Chem. Soc.*, 2003, **125**, 14654.
21. D. Dutta and S. Mishra, *Phys. Chem. Chem. Phys.*, 2014, **16**, 26348.
22. D. Dutta and S. Mishra, *J. Phys. Chem. B,* 2016, **120**, 11654.
23. D. Dutta and S. Mishra, *Phys. Chem. Chem. Phys.*, 2016, **18**, 1671.
24. D. Dutta and S. Mishra, *J. Mol. Graphics Modell.*, 2018, **84**, 82.
25. D. Dutta and S. Mishra, *J. Phys. Chem. B,* 2017, **121**, 7075.
26. D. Gillner, N. Armoush, R. C. Holz and D. Becker, *Bioorg. Med. Chem. Lett.*, 2009, **19**, 6350.
27. A. Starus, B. Nocek, B. Bennett, J. A. Larrabee, D. L. Shaw, W. Sae-Lee, M. T. Russo, D. M. Gillner, M. Makowska-Grzyska, A. Joachimiak, *et al., Biochemistry,* 2015, **54**, 4834.
28. B. Nocek, D. Gillner, Y. Fan, R. Holz and A. Joachimiak, *J. Mol. Biol.*, 2010, **397**, 617.
29. D. A. Case, T. E. Cheatham, T. Darden, H. Gohlke, R. Luo, K. M. Merz, A. Onufriev, C. Simmerling, B. Wang and R. J. Woods, *J. Comput. Chem.*, 2005, **26**, 1668.
30. Y. Zhao and D. G. Truhlar, *Theor. Chem. Acc.*, 2008, **120**, 215.
31. G. A. Petersson, A. Bennett, T. G. Tensfeldt, M. A. Al-Laham, W. A. Shirley and J. Mantzaris, *J. Chem. Phys.*, 1988, **89**, 2193.
32. G. A. Petersson and M. A. Al-Laham, *J. Chem. Phys.*, 1991, **94**, 6081.
33. T. Vreven, K. S. Byun, I. Komaromi, S. Dapprich, J. A. Montgomery (Jr.), K. Morokuma and M. J. Frisch, *J. Chem. Theory Comput.*, 2006, **2**, 815.
34. J. P. Ryckaert, G. Ciccotti and H. J. Berendsen, *J. Comput. Phys.*, 1977, **23**, 327.
35. S. H. Northrup, M. R. Pears, C. Lee, J. A. McCammon and M. Karplus, *Proc. Natl. Acad. Sci. USA*, 1982, **79**, 4035.
36. S. Kumar, J. M. Rosenberg, D. Bouzida, R. H. Swendsen and P. A. Kollman, *J. Comput. Chem.*, 1992, **13**, 1011.
37. A. Grossfield, WHAM: an implementation of the weighted histogram analysis method. version 2.0.9; http://membrane.urmc. rochester.edu/content/wham/.
38. M. J. Frisch, G. W. Trucks, H. B. Schlegel, G. E. Scuseria, M. A. Robb, J. R. Cheese-man, G. Scalmani, V. Barone, B. Mennucci, G. A. Petersson, *et al.*, Gaussian 09 Revision A.1. Gaussian Inc., Wallingford CT, 2009.